RESEARCH ARTICLE

BIOMEDICAL DEVICES

A smart mask for exhaled breath condensate harvesting and analysis

Wenzheng Heng[1], Shukun Yin[1], Jihong Min[1], Canran Wang[1], Hong Han[1], Ehsan Shirzaei Sani[1], Jiahong Li[1], Yu Song[1], Harry B. Rossiter[2], Wei Gao[1]*

Recent respiratory outbreaks have garnered substantial attention, yet most respiratory monitoring remains confined to physical signals. Exhaled breath condensate (EBC) harbors rich molecular information that could unveil diverse insights into an individual's health. Unfortunately, challenges related to sample collection and the lack of on-site analytical tools impede the widespread adoption of EBC analysis. Here, we introduce EBCare, a mask-based device for real-time in situ monitoring of EBC biomarkers. Using a tandem cooling strategy, automated microfluidics, highly selective electrochemical biosensors, and a wireless reading circuit, EBCare enables continuous multimodal monitoring of EBC analytes across real-life indoor and outdoor activities. We validated EBCare's usability in assessing metabolic conditions and respiratory airway inflammation in healthy participants, patients with chronic obstructive pulmonary disease or asthma, and patients after COVID-19 infection.

Respiratory epidemics and pandemics have emphasized the urgent and critical need for comprehensive research on the respiratory system. A number of clinically meaningful molecular analytes such as volatile organic compounds (VOCs, e.g., acetone and alkanes), inorganic substances (e.g., nitric oxide and ammonia), cytokines, and pathogens (e.g., severe acute respiratory syndrome coronavirus 2) are exhaled in the form of gases, aerosols, or droplets (*1*–*3*). The real-time and continuous analysis of exhaled breath biomarkers could theoretically provide immense potential for offering valuable insights into the early diagnosis, monitoring, and management of a variety of respiratory and metabolic health conditions, including asthma (*4*), chronic obstructive pulmonary disease (COPD) (*5*), COVID-19 (*6*), lung cancer (*7*), tuberculosis (*8*), and beyond (*3*). Despite this promise, however, the tools available for studying human breath remain severely restricted. Existing methods of real-time and wireless monitoring of exhaled breath molecular biomarkers are primarily limited to breath alcohol tests, and "electronic noses" based on gas sensors, although actively researched, are limited by inadequate selectivity for practical exhaled breath analysis (*9*–*11*).

Exhaled breath condensate (EBC) is a highly promising noninvasive aqueous matrix in which soluble gaseous and nonvolatile biomarkers can be measured selectively for personalized health care (Fig. 1A) (*2*, *12*). Clinically, EBC is collected using a commercial condenser (*13*) or specialized condensation instruments (*12*, *14*, *15*) and subsequently analyzed in laboratory settings by means of mass spectrometry or photometric assays to assess airway inflammation and substance metabolism (fig. S1) (*16*–*18*). The implementation of these approaches for at-home remote sensing is hindered by challenges related to labor, time, money, and energy costs. Furthermore, issues such as the degradation of reactive substances [e.g., nitrite (NO_2^-) and hydrogen peroxide (H_2O_2)] during the sampling process and storage, interference of oral ingredients, and the absence of continuous dynamic information impede the practical and widespread application of EBC testing (*2*). The recent development of wearable biosensors has ushered in a new era of telehealth, enabling continuous and wireless molecular monitoring of biomarkers in sweat, saliva, and interstitial fluid (*19*–*21*). The exploration of wearable EBC analysis has been limited, however, primarily because of the challenges in condensing exhaled breath, EBC sampling, and in situ analysis during an individual's daily activities (*22*). Face masks are an ideal wearable platform for personal protection (*6*, *23*, *24*) and breath sampling (*25*, *26*). Recent advances in exhaled breath aerosol (EBA) devices based on masks have shown some promise in point-of-care analysis, but their reliance on external media for sample extraction has introduced challenges in terms of stability and reproducibility, which limits their suitability for continuous monitoring (fig. S1 and table S1) (*27*–*29*).

Here, we introduce a mechanically soft microfluidic smart mask system, which we call EBCare (exhaled breath condensate ana[illegible] and respiratory evaluation), designed for [illegible]tinuous exhaled breath condensation, automatic EBC capturing and transport, and real-time in situ EBC biomarker analysis (Fig. 1, A to C; fig. S2; and table S2). Compared to bulky traditional EBC collection devices that rely heavily on ice buckets or refrigeration, EBCare is capable of effective condensation of breath vapor in both indoor and outdoor environments through tandem passive cooling technologies that integrate hydrogel evaporative cooling, metamaterial radiative cooling, and a device framework with high thermal conductivity. A bioinspired microfluidic module substantially enhances EBC harvesting and transport efficiency by leveraging the capillary action driven by surface hydrophilicity and a microengineered graded pillar array (Fig. 1, B and C, and fig. S3). EBCare supports high-temporal-resolution EBC harvesting and transport, making it ideal for real-time continuous in situ analysis (table S1). The EBCare system enables highly sensitive, selective, and continuous EBC biomarker analysis, facilitated by a nanoengineered electrochemical sensor array coupled with a flexible printed circuit board (FPCB) for signal processing and wireless communication (Fig. 1, D and E). The post-analysis EBC efflux is absorbed by a cooling hydrogel, ensuring a continuous water replenishment for sustainable evaporative cooling.

The tandem cooling strategy for exhaled breath condensation

EBC harvesting plays a foundational role in achieving real-time and continuous EBC biomarker analysis with high temporal resolution. To efficiently cool down the condensing surface temperature to the dew point of the exhaled breath in diverse real-life indoor and outdoor scenarios, EBCare uses a tandem passive cooling strategy combining hydrogel evaporation and radiative cooling (Fig. 2, A and B). The main structural framework of EBCare uses a ceramic alumina-polymer hybrid metamaterial with high thermal conductivity and ideal radiative cooling properties (Fig. 2C), comprising micrometer-sized aluminum oxide (Al_2O_3) spheres distributed evenly in a polymeric matrix containing polydimethylsiloxane (PDMS) and copolymer PDMS-block-polyethylene glycol (PDMS-b-PEG) (figs. S4 and S5) (*30*, *31*).

During operation in ambient conditions, the natural evaporation of water from the agarose hydrogel absorbs surrounding heat, substantially reducing the temperature of the hydrogel (*32*). The addition of Ag nanoparticles into the hydrogel both introduced a high antibiotic effect and enhanced EBCare's biocompatibility during long-term on-body use (fig. S6). Simulating the heat from breath with a heating source (fig. S7A) demonstrated that

[1]Andrew and Peggy Cherng Department of Medical Engineering, Division of Engineering and Applied Science, California Institute of Technology, Pasadena, CA, USA. [2]Division of Respiratory and Critical Care Physiology and Medicine, Institute for Respiratory Medicine and Exercise Physiology, The Lundquist Institute for Biomedical Innovation at Harbor-UCLA Medical Center, Torrance, CA, USA.
*Corresponding author. Email: weigao@caltech.edu

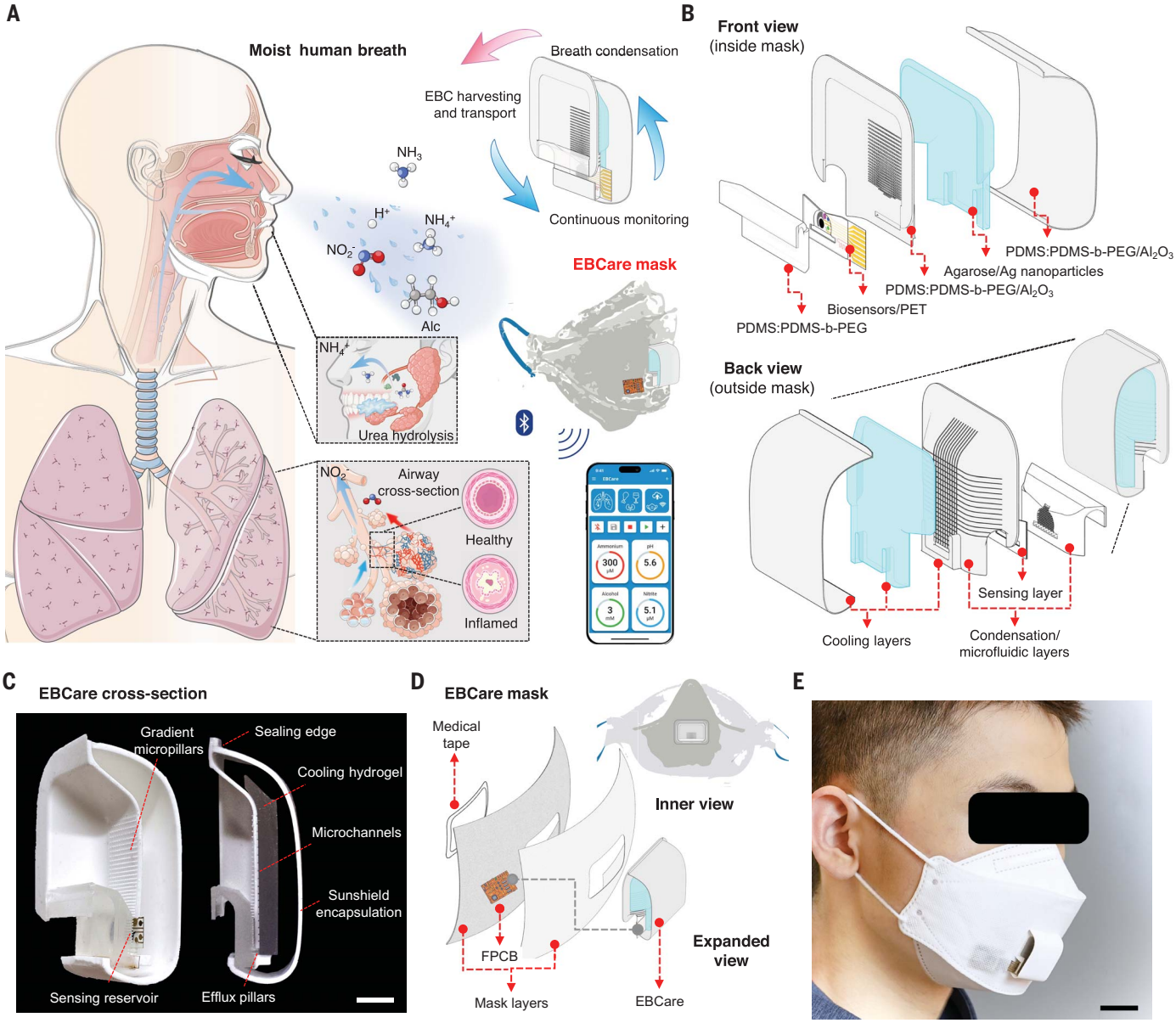

Fig. 1. A smart EBCare (exhaled breath condensate analysis and respiratory evaluation) mask for efficient harvesting and continuous analysis of exhaled breath condensate. (**A**) EBCare is capable of exhaled breath condensation, EBC harvesting and transport, and continuous analysis of biomarkers from the human respiratory tract. Alc, alcohol. (**B** and **C**) Exploded-view schematic illustration (B) and cross-sectional optical images (C) of the main components of an EBCare device. Scale bar, 4 mm. PDMS, polydimethylsiloxane; PEG, polyethylene glycol; PET, polyethylene terephthalate. (**D**) Schematic showing the expanded and inner views of the smart mask integrated with an EBCare device. FPCB, flexible printed circuit board. (**E**) Photograph of a fully integrated wireless smart mask worn by a participant. Scale bar, 3 cm.

hydrogel evaporation effectively reduces the surface temperature by 4° to 14°C under varied relative humidity (RH) and ambient temperature (Fig. 2D). In a standard indoor environment (23°C and 50% RH), the temperature of the heating source was controlled to be similar to the temperature of human breath, and hydrogel evaporation induced a temperature drop of ~8°C, well below the dew point of the exhaled breath (~5°C below breath temperature under 75% RH) (Fig. 2D). However, without continuous liquid replenishment, the evaporative cooling function of the hydrogel diminished substantially after 2 to 3 hours (figs. S7B and S8A and movie S1). Introducing a condensate circulation system that transports the continuously harvested EBC to the hydrogel ensured sustainable and stable evaporative cooling for at least 7 hours (figs. S7, C and D, and S8).

On sunny days, under strong solar radiation, the potential elevation of EBCare temperature as a result of the hydrogel absorbing sunlight could compromise breath condensation during outdoor wearing (*33*). To address this issue, a tandem radiative cooling function was integrated into the device design using metamaterial PDMS:PDMS-b-PEG/Al_2O_3 as the main EBCare framework and sunshield layer. Owing to the Mie scattering of spherical alumina microparticles under solar spectrum and the strong emission properties of polymeric matrix in the mid-infrared (MIR) region, the hybrid polymeric metamaterial achieved ~95% solar reflectivity and ~95% MIR thermal emissivity (Fig. 2C and fig. S9). Such

optical properties effectively reduce the solar radiation absorption and radiate heat through the MIR range in the atmospheric window to outer space, ensuring the high efficiency of the condensation process even under strong sunlight exposure in outdoor environments.

EBCare's tandem cooling effects were evaluated in both indoor and outdoor environments during the day and at night and were compared with normal fabric mask material without a cooling function and materials with only one type of cooling method (stand-alone exposed hydrogel and PDMS:PDMS-b-PEG/Al_2O_3 framework) (Fig. 2E, fig. S10, and movie S2). The EBCare device demonstrated a temperature ~7°C lower than radiative cooling material alone and ~10°C lower than nonradiative cooling mask material throughout the indoor and outdoor tests at night. The cooling effect was more substantial under 1 sun (~1 kW m^{-2}) radiation, with a temperature ~5°C lower than the exposed hydrogel and ~15° and ~20°C below those of the radiative cooling layer and nonradiative cooling mask layer, respectively (fig. S11). The cooling system design of EBCare was further validated by comparing EBC collection results of these materials from healthy participants under daily indoor and outdoor environments (Fig. 2F, fig. S12, and table S3). EBCare's collection rate was five times greater than that without cooling under indoor conditions and twice as great as exposed hydrogel cooling alone under outdoor conditions. Even under 1 sun flux, the device still captured EBC at a high rate of around 4 μl min^{-1}, indicating highly efficient,

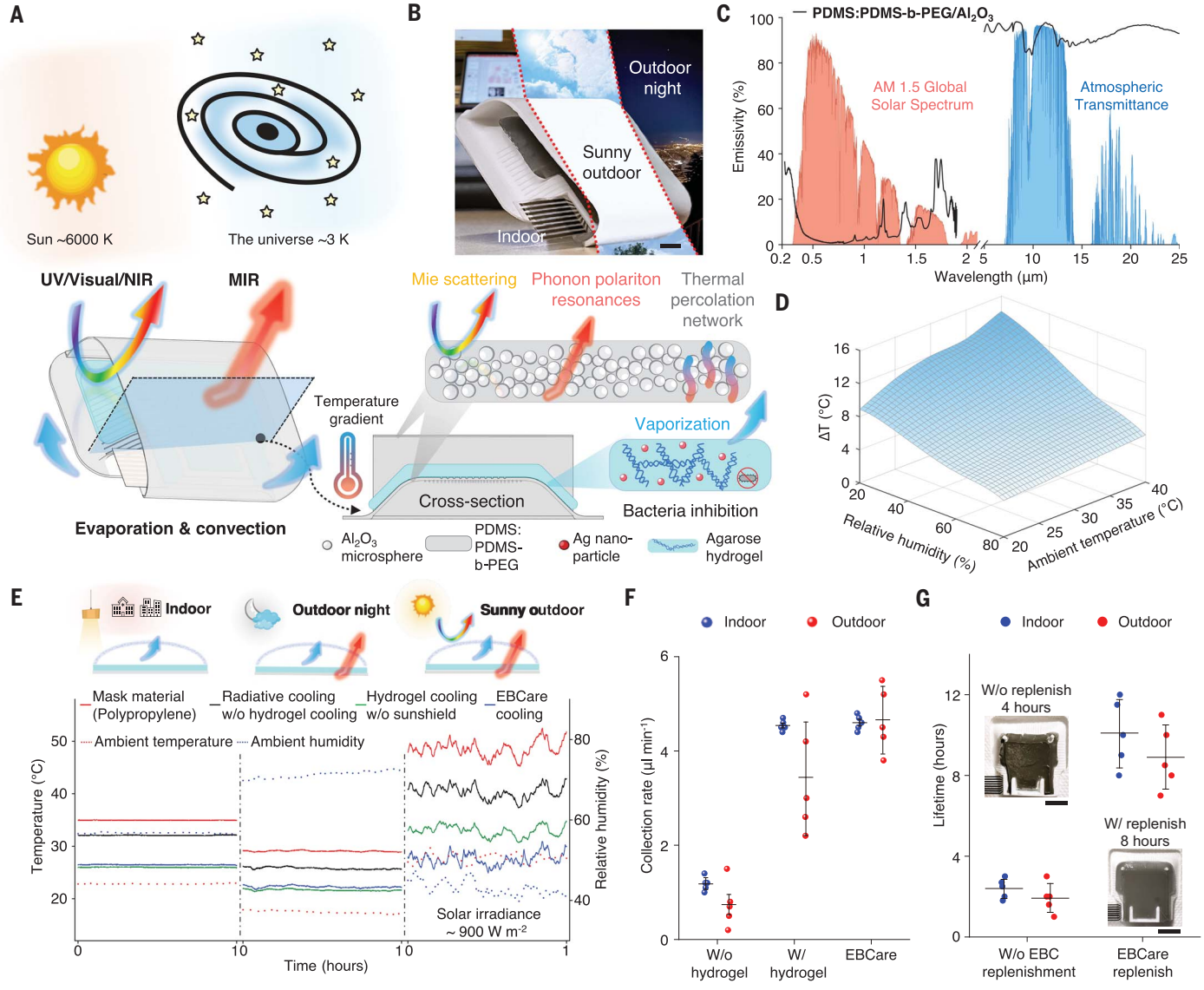

Fig. 2. Characterization of EBCare's tandem cooling design for breath condensation. (**A**) Schematic of an EBCare device with simultaneous indoor and outdoor cooling capabilities for efficient breath condensation. UV, ultraviolet; NIR, near infrared; MIR, mid infrared. (**B**) Photographs of an EBCare device in indoor, sunny outdoor, and outdoor night settings. Scale bar, 5 mm. (**C**) Spectral emissivity of a polymeric metamaterial film (0.5 mm thick). Red and blue colors represent AM 1.5 solar spectrum and the atmospheric window, respectively. (**D**) Cooling capacity of the hydrogel under varied ambient RH and temperature. Δ*T*, surface temperature drops in the presence of hydrogel. (**E**) Surface temperature of different cooling strategies under indoor and outdoor (at night and in sunlight) environments. (**F**) EBC harvesting performance of different cooling strategies from a healthy participant. (**G**) Hydrogel lifetime for the EBCare device with and without EBC refreshing. Insets show the hydration state of the hydrogel on EBCare with and without EBC refreshing. Scale bars, 1 cm. All error bars in the figure represent standard deviations of the mean.

continuous, and long-term EBC condensation through the tandem passive cooling strategy (Fig. 2, F and G).

Bioinspired microfluidics for EBC sampling, transport, and refreshing

The continuous respiratory monitoring capability of the EBCare mask system hinges on the self-directed flow of EBC within an integrated bioinspired microfluidic system. The natural conveyance of water and chemicals in plants primarily relies on the capillary phenomenon (fig. S13). In plants, water transpires from the stomata of leaves, transforming into water vapor. This process induces a reduction of water content inside the leaves, creating negative pressure inside the plant's diminutive hydrophilic xylem vessels. Consequently, water is drawn upward from the ground through the capillary forces to meet the plant's water needs (*34*). Inspired by this biological process, EBCare's microfluidic module incorporates micropillars with structural gradients, hydrophilic microfluidic channels, and evaporative cooling hydrogels, serving as the graded capillary pumps for gravity-independent EBC sampling, transport, and refreshing (Fig. 3A).

The hydrophilic interface of the EBCare device's inner surface, which is similar to xylem vessels, is crucial for enabling the automatic circulation of harvested EBC through microfluidics. In our study, increasing the doping ratio of the copolymer PDMS-b-PEG to 1% in EBCare's main framework material (PDMS: PDMS-b-PEG/Al_2O_3) substantially enhanced hydrophilicity, achieving a low contact angle of 15.5° owing to an increased C-O bond surface distribution (Fig. 3B and figs. S14 and S15) (*35*). Unlike plasma-treated pristine PDMS, which can lose its hydrophilicity within hours, the hybrid polymer PDMS:PDMS-b-PEG/Al_2O_3 was able to maintain high hydrophilicity over a 1-month period (fig. S16). This hydrophilic nature, in contrast to hydrophobic surfaces, offers advantages in terms of EBC nucleation, cohesion, and collection (fig. S17) (*36*). Such a hybrid material also exhibits excellent biological anti-adhesive and nonfouling properties, making it ideal for EBC sampling and subsequent in situ bioanalysis with high accuracy (fig. S18) (*37*).

The spontaneous and highly efficient directional transport of EBC to the sensing reservoir, after EBC capture at the hydrophilic

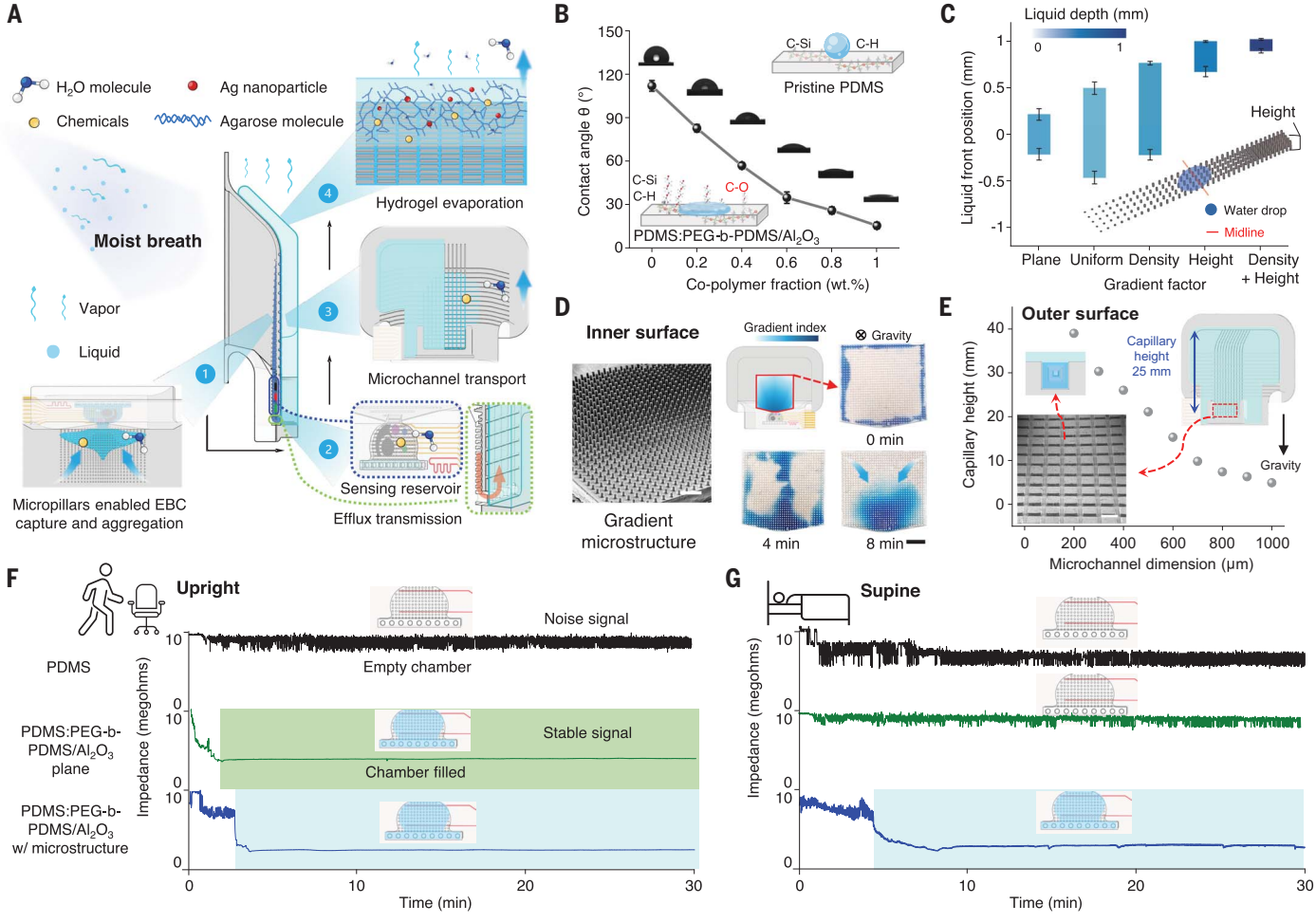

Fig. 3. Characterization of the microfluidic design of the EBCare device for EBC sampling, transport, and refreshing. (**A**) Schematic of the microfluidic design of the EBCare device for EBC sampling, transport, and refreshing. (**B**) Contact angle of PDMS:PDMS-b-PEG/Al_2O_3 with varied mass fractions of the PDMS-b-PEG copolymer. (**C**) Comparison of the unidirectional liquid transport capacity of the prewetted micropillar array designs with varied gradient factors (density and height). (**D**) Scanning electron microscopy (SEM) image (left) of the micropillar structure at the inner surface of EBCare, and schematic and top-down–view snapshots (right) of liquid transport on the inner surface of EBCare. Gravity perpendicular to surface and inward. Scale bars, 1 mm (left) and 3 mm (right). (**E**) Height of capillary water transport for hydrogel refreshing on the outer surface of EBCare. Insets show microchannel cross-sectional schematic (top left), SEM image (bottom left), and capillary pumping schematic (top right) of the outer surface structure. Scale bar, 1 mm. (**F** and **G**) Impedance between a pair of electrodes in the sensing reservoir obtained using EBCare devices with varied inner surface properties (hydrophilicity, with or without microstructures) for participants under upright (F) and supine (G) conditions for verifying the presence of EBC in the sensing chamber. All error bars in the figure represent standard deviations of the mean.

inner surface of EBCare device, was facilitated by the graded capillary forces resulting from an array of micropillars with both height and density gradients (Fig. 3, C and D; figs. S19 to S21; and movies S3 and S4). The stabilized EBC continuously flows through the sensing reservoir, where it is analyzed by the built-in electrochemical sensors. Subsequently, driven by strong capillary forces from hydrogel-covered microchannels on EBCare's outer surface, EBC is automatically transferred to the device's outer surface through efflux columns between the inner and outer interfaces and transports effectively against gravity via microfluidic channels (Fig. 3E). EBC is then absorbed by the hydrogel along with the hydrogel evaporation, providing a continuous water source for hydrogel evaporative cooling.

The in vitro assessment of the fully assembled microfluidic system demonstrated efficient liquid harvesting, transport, effluxion, and evaporation, paving the way for sustainable wearable EBC analysis (figs. S22 and S23 and movies S5 and S6). By incorporating an impedimetric sensor into the sensing reservoir, we evaluated the EBC sampling capabilities of EBCare in healthy participants by considering different inner surface materials and structures (Fig. 3, F and G). The results revealed that the device made of pristine PDMS was not capable of sampling EBC into the sensing reservoir under both upright and supine conditions owing to the hydrophobic surface. The device with planar hydrophilic PDMS:PDMS-b-PEG/Al_2O_3 was only able to access EBC under upright conditions, where gravity served as the driving force. In contrast, the EBCare device, constructed from hydrophilic PDMS:PDMS-b-PEG/Al_2O_3 with graded microstructures, demonstrated the ability to harvest and transport EBC into the sensing reservoir within 5 min even in supine postures. Stable and continuous wearable EBC analysis is possible under various real-life conditions, including gravity-defying supine positions, where graded capillary forces acted as the primary driving force (fig. S24 and movie S7). On the basis of the optimized design, EBCare's start-up time for in situ EBC analysis is estimated at only 3 min when in an upright posture (fig. S25). Our tests further indicated that the EBCare device can efficiently harvest EBC from human participants at rates as high as ~5 $\mu l\ min^{-1}$ (fig. S26). This rate is sufficient for high-temporal-resolution EBC analysis, given the small volume of the sensing reservoir (~5 μl) (fig. S27). Additionally, EBCare can be easily integrated into various types of face masks for efficient EBC sampling (fig. S26), thanks to its high mechanical flexibility and stretchability (fig. S28). It should be noted that placing EBCare above the upper lip when integrated with a face mask effectively mitigates saliva contamination in EBC sampling, as confirmed by saliva amylase tests on collected EBCs (fig. S29). In cases of transient or long-term coughing, saliva contamination effects on EBC analyte concentration can be eliminated within a few minutes through microfluidic refreshing, as demonstrated in simulations and on-body test results (fig. S30).

Wireless electrochemical biosensor array for multiplexed EBC analysis

To demonstrate the wearable applications of EBCare, we integrated an electrochemical sensor array into the smart mask for simultaneous and multiplexed in situ EBC analysis. The mechanically flexible and disposable sensor array included amperometric nitrite (NO_2^-) and alcohol sensors, potentiometric ion-selective pH and NH_4^+ sensors, and a resistive temperature sensor (Fig. 4A). The electrochemical sensor can be mass-produced at low cost through inkjet printing on a flexible substrate such as polyethylene terephthalate (PET). EBC is characterized as a highly diluted solution with low ionic strength with NH_4^+ dominating the EBC cation composition, reflecting its electrical conductivity (fig. S31) (*38*). We have designed our sensors in such a way as to optimize their performance for EBC analysis. This includes ensuring a linear range that accommodates physiological concentrations and maintaining stability in matrices with low ionic strength (figs. S32 to S34). The target analytes were selected on the basis of their clinical significance, with alcohol detection facilitated by an alcohol oxidase–modified Pt-decorated Au electrode, nitrite quantification based on selective oxidation under the applied redox potential (0.75 V) on the inkjet-printed carbon nanoparticle electrode (outperforming commercially available screen-printed and glassy carbon electrodes, as illustrated in fig. S33), and pH and NH_4^+ sensing based on pH-responsive polyaniline film and NH_4^+-selective membrane-modified electrodes, respectively.

Electrochemical characterization of each EBC biosensor in standard solutions containing analyte with physiologically relevant concentrations revealed linear responses between the measured current signals and the target concentrations for alcohol and NO_2^- and between the measured voltage signals and the logarithmic target concentrations for pH and NH_4^+ sensors (Fig. 4, B to E, and fig. S34). All biosensors exhibited high selectivity in simulated EBC against potential interference analytes (fig. S35). While pH and NH_4^+ concentration in EBC provide clinically relevant information, they can also act synergistically to calibrate the alcohol and nitrite sensors (fig. S36). Additionally, real-time temperature information from the integrated carbon-based resistive temperature sensor contributes to further sensor calibration during wearable device use (fig. S37). With these calibration mechanisms, the electrochemical NH_4^+ and NO_2^- sensors demonstrated high accuracy for human EBC analysis, validated against commercial assay kits (Fig. 4F).

To realize wireless multiplexed wearable EBC analysis, an FPCB was designed for multimodal electrochemical measurements (e.g., voltammetry, potentiometry, and impedimetry), signal processing, and wireless communication (Fig. 4G, figs. S38 and S39, and table S4). Real-time collected analyte information can be transmitted to a user interface through Bluetooth Low Energy (BLE) and displayed on a custom-developed mobile app (movie S8). As EBCare uses a multiplexed circuit for continuous monitoring, the sampling rate can be programmatically adjusted to any desired frequency below 100 Hz. To balance the data processing load and the time-varying nature of the selected biomarkers, an analysis period of 3.6 s was chosen for on-body tests (fig. S40). EBCare features three operational modes to optimize power consumption: running mode, low-power mode, and lower-power intermittent mode. These modes adjust the electrochemical measurement and data collection processes, enabling efficient, long-term continuous sensing (table S4 and fig. S41). The fully integrated EBCare accurately and simultaneously monitored dynamic responses of the integrated NO_2^-, alcohol, NH_4^+, pH, and temperature sensors; all biosensors exhibited high stability during continuous microfluidic sensing and high selectivity to other interferent molecules, showcasing great promise for in situ wearable EBC analysis (Fig. 4H). For the integrated EBCare system, the cost of the reusable FPCB is ~$40, and the disposable sensor patch and microfluidic components each cost around $0.60 (table S5).

Evaluation of EBCare in healthy and patient participants for personalized medicine

To evaluate EBCare's long-term usability for continuous EBC sampling and analysis in daily-life scenarios, we studied a healthy individual over a time span of 14 hours, tracking activities such as exercise, eating and drinking, office work, and napping (Fig. 5A). After breakfast, EBC NH_4^+ concentration initially slightly decreased, then increased, and then rose more substantially after lunch and dinner, both of which involved a larger amount of protein intake. Associations between changes in EBC pH and NH_4^+ concentration were attributed to the ammonium bicarbonate buffer matrix in the EBC. Additionally, alcohol intake with meals led to rapid elevation of EBC alcohol concentration, consistent with the dynamics of alcohol metabolism. Throughout the day, EBC NO_2^- in the healthy individual remained relatively stable at low levels.

Multiple human studies were performed to demonstrate that the analyte information

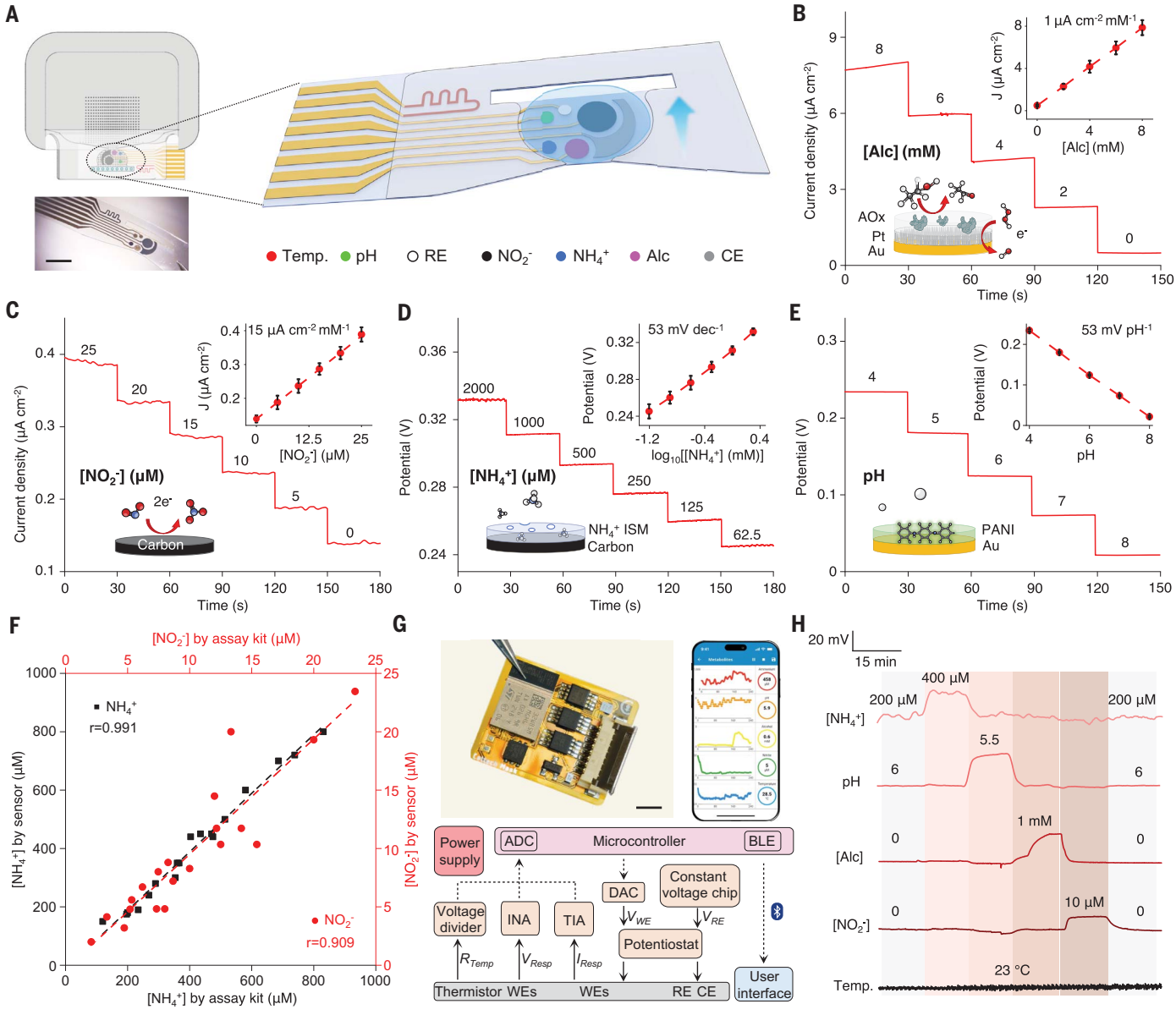

Fig. 4. Design and characterization of the wireless electrochemical biosensor array for in situ multiplexed EBC analysis. (**A**) Schematic and optical image of an inkjet-printed electrochemical sensing array for simultaneous in situ multiplexed monitoring of EBC NH_4^+, pH, alcohol, NO_2^-, and temperature. RE, reference electrode; CE, counter electrode. (Inset) Photo of a flexible inkjet-printed electrochemical sensor array. Scale bar, 5 mm. (**B** and **C**) Amperometric responses of an enzymatic alcohol sensor (B) and a NO_2^- sensor (C) in artificial EBC (400 μM NH_4HCO_3) containing varied analyte concentrations. (Insets) The corresponding calibration plots (top right) and schematic (bottom left) of the alcohol and NO_2^- sensors. J, current density; AOx, alcohol oxidase. (**D** and **E**) Open circuit potential responses of an ion-selective NH_4^+ sensor (D) and a polyaniline-based pH sensor (E) in standard analyte solutions. (Insets) The corresponding calibration plots (top right) and schematic (bottom left) of the NH_4^+ and pH sensors. ISM, ion-selective membrane; PANI, polyaniline. (**F**) Validation of the NH_4^+ and NO_2^- sensors against commercial assay kits for analyzing collected EBC samples from participants (n = 15 biological replicates from N = 5 healthy participants). (**G**) Image and schematic diagram of the integrated electronic system and mobile app for wireless EBC analysis. ADC, analog-to-digital converter; BLE, Bluetooth Low Energy; DAC, digital-to-analog converter; INA, instrumentation amplifier; TIA, transimpedance amplifier; WE, working electrode. Scale bar, 3 mm. (**H**) System-level multiplexed interference study of the electrochemical biosensor array in a microfluidic test. All error bars in the figure represent standard deviations of the mean.

collected by EBCare from human participants holds potential for a broad spectrum of personalized health care applications (Fig. 5B). For example, nasal EBC alcohol concentration analyzed using EBCare after alcohol consumption exhibited strong correlation with blood alcohol concentration (BAC)—the gold standard for monitoring alcohol metabolism or assessing driving under the influence (Fig. 5C). In contrast to the standard mouth blow–based BAC tests, which provide discrete information and are susceptible to contamination from alcohol-containing salivary droplets in the oral cavity, EBCare represents a solution for continuous, accurate, and real-time alcohol metabolism monitoring (*39*).

Through a series of protein challenge studies in healthy individuals using in situ real-time analysis with EBCare masks and in vitro analysis with collected human EBC samples, we identified elevated NH_4^+ concentration in EBC,

alongside increased serum urea concentration (Fig. 5D and figs. S42 to S44). Controlled low- or high-protein diets in a healthy individual over a 2-week period resulted in similar dynamic patterns between EBC NH_4^+ and serum urea concentrations (fig. S45). A linear correlation between the EBC NH_4^+ and serum urea concentration was obtained with a correlation coefficient (r) of 0.846 (Fig. 5E). These findings

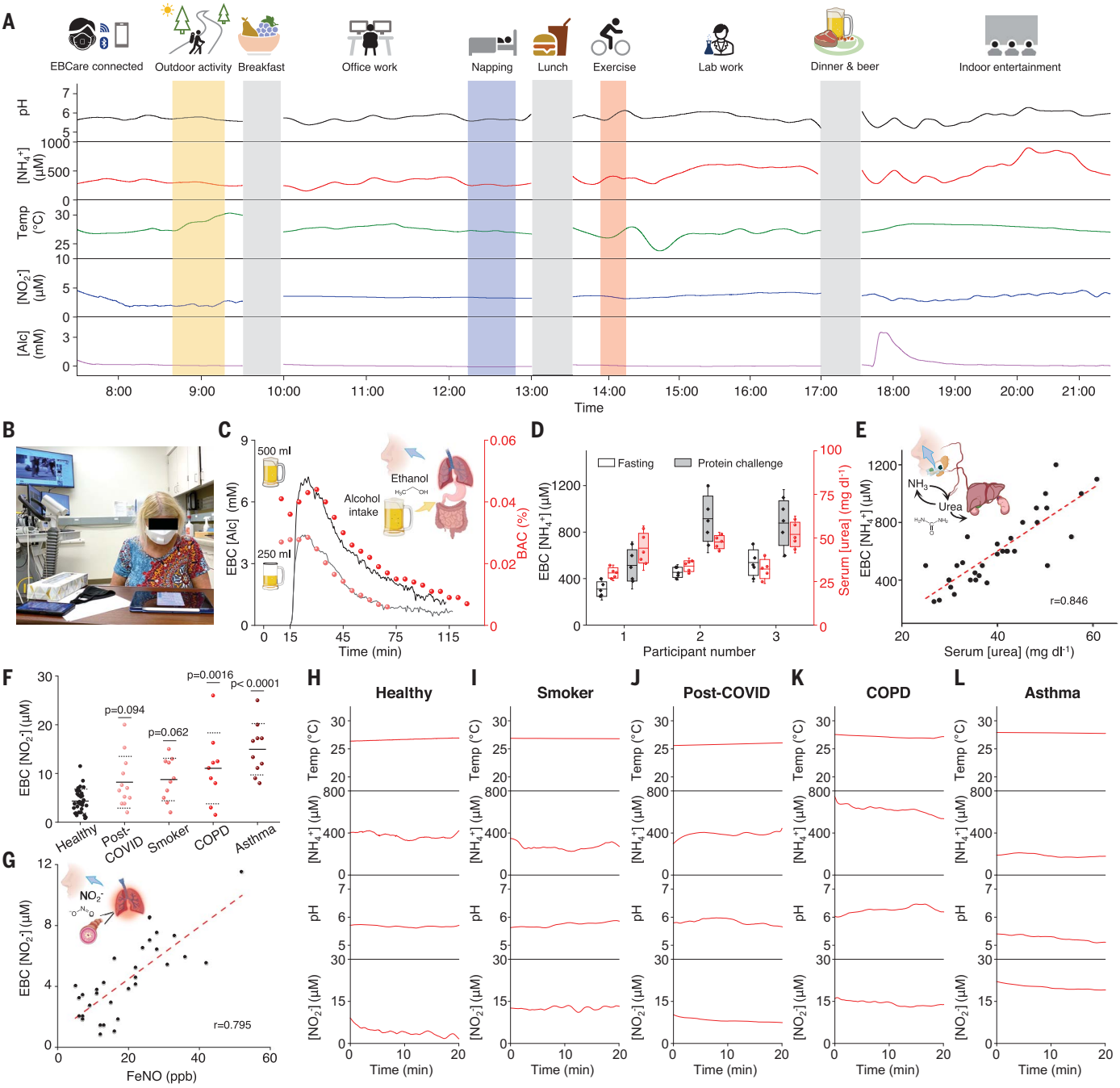

Fig. 5. On-body evaluation of EBCare for EBC analysis in healthy and patient populations. (**A**) Full-day cross-activity in situ EBC analysis of a healthy participant with EBCare monitoring. (**B**) Photograph of a COPD patient wearing an EBCare mask during a clinical study. (**C**) Breath alcohol concentration monitored by EBCare mask from a healthy participant versus BAC breath test after consumption of different doses of alcohol. (**D**) Evaluation of EBCare during a protein challenge: EBC NH_4^+ and serum urea concentrations (n = 15 biological replicates from N = 3 healthy participants) before and after consuming 120 g of protein in a day. (**E**) The correlation between EBC NH_4^+ and serum urea concentration (n = 35 biological replicates from N = 5 healthy participants). (**F**) EBC NO_2^- concentration in participants with or potentially with airway inflammation (n = 72 biological replicates from N = 31 healthy controls, N = 12 individuals newly recovered from COVID-19, N = 10 current smokers, N = 9 patients with COPD, and N = 10 patients with asthma). Statistical analysis of EBC NO_2^- concentration: one-way analysis of variance and Tukey's post hoc test. (**G**) The correlation between EBC NO_2^- and fractional exhaled nitric oxide (FeNO) (n = 31 biological replicates from 31 independent participants). ppb, parts per billion. (**H** to **L**) On-body multiplexed EBC analysis with real-time sensor calibrations using the EBCare mask on a healthy participant (H), a current smoker (I), an individual newly recovered from COVID-19 (J), a patient with COPD (K), and a patient with asthma (L). All error bars in the figure represent standard deviations of the mean.

suggest that the EBC NH_4^+ is derived from oral saliva urea degradation and has the potential to serve as a noninvasive alternative biomarker for serum urea in renal disease management and personalized protein metabolism monitoring (*40*, *41*).

The clinical utility of the EBCare mask-enabled EBC analysis was evaluated in patients with respiratory diseases such as COPD and asthma and after COVID-19 infection (Fig. 5F, fig. S46, and tables S6 to S8). Given the commonality of airway inflammation in respiratory diseases, we first investigated the concentration of EBC NO_2^- using the EBCare mask in individuals categorized by airway inflammation type: healthy control (n = 31), smokers (n = 10), participants newly recovered from COVID-19 (n = 12), patients with COPD (n = 9), and patients with asthma (n = 10), where NO_2^- is a representative marker of reactive nitrogen species (*42*). Elevated EBC NO_2^- concentration was observed in groups with airway inflammation, particularly asthma groups ($P < 0.0001$), surpassing concentrations in the healthy control group (Fig. 5F and fig. S47), highlighting the potential for EBC NO_2^- in the diagnosis, monitoring, and management of patients with respiratory airway inflammation (*43*, *44*). Our studies, which included physical experiments (fig. S48) and patient questionnaires (table S9 and fig. S49), also demonstrated the high breathability and comfort of the EBCare mask, even for patients experiencing breathing difficulties.

To further demonstrate the clinical significance of EBC NO_2^- for asthma and other respiratory disease management, we validated our sensors' results against a clinically well-recognized biomarker, fractional exhaled nitric oxide (FeNO), often referred to as an "inflammometer" (*45*). FeNO has demonstrated promise in identifying type 2 inflammation in asthma and in the management of allergic asthma (*46*–*48*), serving as a crucial indicator of lung inflammation levels and the effectiveness of inhaled steroid treatment (*47*, *49*, *50*). Our study revealed a robust r of 0.795 between EBC NO_2^- and FeNO across a cohort of 31 human subjects (Fig. 5G).

Multiplexed sensor data collected by the EBCare mask from individuals with varying health conditions revealed rich personalized health information at the molecular level (Fig. 5, H to L, and figs. S50 to S52). Beyond inflammatory conditions reflected by EBC NO_2^-, elevated EBC NH_4^+ in COPD patients potentially indicates a higher serum urea, and a lower EBC pH may be related to airway acidification in asthma patients (*2*).

Conclusions

Unlike traditional time-consuming laboratory EBC tests or wearable biosensors analyzing sweat or saliva, EBCare enables continuous collection of intricate molecular information from exhaled breath with high selectivity and temporal resolution. Incorporated seamlessly into everyday face masks, EBCare uses a powerless tandem cooling strategy for stable and continuous exhaled breath condensation, a preprogrammed capillary force gradient design ensuring automatic sampling and refreshing of EBC, and a disposable multiplexed electrochemical biosensor array for in situ dynamic monitoring of exhaled breath biomarkers with high accuracy during daily activities. EBCare introduces a dynamic, user-friendly, and real-time detection platform that overcomes complex challenges such as saliva contamination, ongoing monitoring, wearable tracking, extended analysis periods, nasal breath condensate collection, and cost-effective surveillance in the traditional clinical EBC field.

Our pilot human trials involving healthy individuals and patients with diagnosed COPD, asthma, or COVID-19 underscore the potential of EBC and EBCare for personalized assessment of metabolic and inflammatory conditions. Moreover, EBCare's adaptability allows for the monitoring of various clinically relevant molecules in the EBC through electrochemical analysis. The significance of EBCare lies in its role as a versatile, convenient, efficient, real-time research platform and solution in various medical domains, providing a robust and effective tool for this kind of future-advancing clinical and medical studies.

REFERENCES AND NOTES

1. C. C. Wang *et al.*, *Science* **373**, eabd9149 (2021).
2. I. Horváth *et al.*, *Eur. Respir. J.* **26**, 523–548 (2005).
3. W. Ibrahim *et al.*, *Sci. Transl. Med.* **14**, eabl5849 (2022).
4. R. A. Dweik *et al.*, *Am. J. Respir. Crit. Care Med.* **184**, 602–615 (2011).
5. P. J. Barnes, *J. Allergy Clin. Immunol.* **138**, 16–27 (2016).
6. N. H. L. Leung *et al.*, *Nat. Med.* **26**, 676–680 (2020).
7. G. Peng *et al.*, *Nat. Nanotechnol.* **4**, 669–673 (2009).
8. S. F. Mosquera-Restrepo *et al.*, *Nat. Commun.* **13**, 7751 (2022).
9. F. Röck, N. Barsan, U. Weimar, *Chem. Rev.* **108**, 705–725 (2008).
10. U. Yaqoob, M. I. Younis, *Sensors* **21**, 2877 (2021).
11. S. Y. Park *et al.*, *InfoMat* **1**, 289–316 (2019).
12. J. Hunt, *J. Allergy Clin. Immunol.* **110**, 28–34 (2002).
13. E. M. Konstantinidi, A. S. Lappas, A. S. Tzortzi, P. K. Behrakis, *ScientificWorldJournal* **2015**, 435160 (2015).
14. M. Khorshid *et al.*, *Adv. Sens. Res.* **3**, 2400020 (2024).
15. X. Chen *et al.*, *Microchem. J.* **198**, 110130 (2024).
16. P. Kubáň, F. Foret, *Anal. Chim. Acta* **805**, 1–18 (2013).
17. P. Montuschi, *Clin. Chim. Acta* **356**, 22–34 (2005).
18. N. Hashemzadeh, E. Rahimpour, A. Jouyban, *J. Pharm. Pharm. Sci.* **25**, 391–401 (2023).
19. W. Gao *et al.*, *Nature* **529**, 509–514 (2016).
20. H. C. Ates *et al.*, *Nat. Rev. Mater.* **7**, 887–907 (2022).
21. J. Kim, A. S. Campbell, B. E.-F. de Ávila, J. Wang, *Nat. Biotechnol.* **37**, 389–406 (2019).
22. H. C. Ates, C. Dincer, *Nat. Rev. Bioeng.* **1**, 80–82 (2023).
23. A. Yang *et al.*, *Nano Lett.* **17**, 3506–3510 (2017).
24. S. K. Pal, D. Y. Choi, G. Kim, *ACS Appl. Polym. Mater.* **5**, 5888–5895 (2023).
25. X. Liu, B. Hu, *Anal. Bioanal. Chem.* **415**, 3759–3768 (2023).
26. D. Maier *et al.*, *ACS Sens.* **4**, 2945–2951 (2019).
27. P. Q. Nguyen *et al.*, *Nat. Biotechnol.* **39**, 1366–1374 (2021).
28. C. M. Williams *et al.*, *Lancet Infect. Dis.* **20**, 607–617 (2020).
29. H. Li *et al.*, *Nat. Commun.* **14**, 7539 (2023).
30. Y. Zhai *et al.*, *Science* **355**, 1062–1066 (2017).
31. H. Zhang *et al.*, *Proc. Natl. Acad. Sci. U.S.A.* **117**, 14657–14666 (2020).
32. M. Park *et al.*, *Proc. Natl. Acad. Sci. U.S.A.* **120**, e2217828120 (2023).
33. J. Li *et al.*, *Sci. Adv.* **8**, eabq0411 (2022).
34. N. A. Dudukovic *et al.*, *Nature* **595**, 58–65 (2021).
35. M. Yao, J. Fang, *J. Micromech. Microeng.* **22**, 025012 (2012).
36. Y. Wang, W. Zhao, M. Han, J. Xu, K. C. Tam, *Nat. Water* **1**, 587–601 (2023).
37. P. P. Rosias *et al.*, *Eur. Respir. J.* **28**, 1036–1041 (2006).
38. R. M. Effros *et al.*, *Am. J. Respir. Crit. Care Med.* **173**, 386–392 (2006).
39. F. Tehrani *et al.*, *Nat. Biomed. Eng.* **6**, 1214–1224 (2022).
40. L. R. Narasimhan, W. Goodman, C. K. N. Patel, *Proc. Natl. Acad. Sci. U.S.A.* **98**, 4617–4621 (2001).
41. W. Chen, M. Metsälä, O. Vaittinen, L. Halonen, *J. Breath Res.* **8**, 036003 (2014).
42. J. O. Lundberg, E. Weitzberg, M. T. Gladwin, *Nat. Rev. Drug Discov.* **7**, 156–167 (2008).
43. W. Formanek *et al.*, *Eur. Respir. J.* **19**, 487–491 (2002).
44. V. Rihák *et al.*, *J. Clin. Lab. Anal.* **24**, 317–322 (2010).
45. M. W. H. Pijnenburg, J. C. De Jongste, *Clin. Exp. Allergy* **38**, 246–259 (2008).
46. S. Turner, *Curr. Opin. Allergy Clin. Immunol.* **8**, 70–76 (2008).
47. S. Karrasch *et al.*, *Thorax* **72**, 109–116 (2017).
48. N. Murugesan, D. Saxena, A. Dileep, M. Adrish, N. A. Hanania, *Diagnostics (Basel)* **13**, 1428 (2023).
49. Asthma and Allergy Foundation of America, "FeNO tests to monitor FeNO levels"; https://aafa.org/asthma/asthma-diagnosis/lung-function-tests-diagnose-asthma/feno-tests-to-monitor-feno-levels.
50. American Academy of Allergy, Asthma, and Immunology, "What is a FeNO test?"; https://www.aaaai.org/tools-for-the-public/conditions-library/asthma/what-is-a-feno-test.

ACKNOWLEDGMENTS

We gratefully acknowledge critical support and infrastructure provided for this work by the Kavli Nanoscience Institute at Caltech. We acknowledge support from the Beckman Institute of Caltech to the Molecular Materials Research Center and J. Evans for help with x-ray photoelectron spectroscopy. We also thank G. R. Rossman for assistance with Fourier transform infrared spectroscopy MIR spectrum measurement. **Funding:** National Institutes of Health grant R01HL155815 (W.G.); National Institutes of Health grant R21DK13266 (W.G.); National Science Foundation grant 2145802 (W.G.); Office of Naval Research grants N00014-21-1-2483 and N00014-21-1-2845 (W.G.); Army Research Office grant W911NF-23-1-0041 (W.G.); American Cancer Society Research Scholar grant RSG-21-181-01-CTPS (W.G.); the Tobacco Related Disease Research Program grant T31IP1666 (W.G. and H.B.R.); and US Army Medical Research Acquisition Activity grant HT9425-24-1-0249 (W.G. and H.B.R.). **Author contributions:** Conceptualization: W.G. and W.H. Methodology: W.G. and W.H. Investigation: W.H., S.Y., J.M., C.W., H.H., E.S.S., J.L., and H.B.R. Visualization: W.H. and Y.S. Funding acquisition: W.G. and H.B.R. Supervision: W.G. Writing – original draft: W.G. and W.H. Writing – review & editing: all authors. **Competing interests:** H.B.R. is also affiliated with University of Leeds, UK. Additionally, H.B.R. reports consulting fees from the NIH RECOVER-ENERGIZE working group (1OT2HL156812) and is involved in contracted clinical research with Astellas, GlaxoSmithKline, Genentech, Intervene Immune, Mezzion, Novartis, Regeneron, Respira, and United Therapeutics. **Data and materials availability:** All data are available in the main text or the supplementary materials.

SUPPLEMENTARY MATERIALS

science.org/doi/10.1126/science.adn6471
Materials and Methods
Supplementary Text
Figs. S1 to S52
Tables S1 to S9
References (*51*–*72*)
Movies S1 to S8

Submitted 20 December 2023; resubmitted 31 May 2024
Accepted 17 July 2024
10.1126/science.adn6471